

Dysfunction of ubiquitin protein ligase *MYCBP2* leads to cell resilience in human breast cancers

Ryan A. Neff^{1,2,3,4,†}, Almudena Bosch-Gutierrez^{1,5,6,†}, Yifei Sun^{1,5,6,†}, Igor Katsyv⁷, Won-min Song^{1,2,3}, Minghui Wang^{1,2,3}, Martin J. Walsh^{1,5,6,*} and Bin Zhang^{1,2,3,5,*}

¹Department of Genetics and Genomic Sciences, Icahn School of Medicine at Mount Sinai, One Gustave L. Levy Place, New York, NY 10029, USA, ²Mount Sinai Center for Transformative Disease Modeling, Icahn School of Medicine at Mount Sinai, One Gustave L. Levy Place, New York, NY 10029, USA, ³Icahn Institute for Data Science and Genomic Technology, Icahn School of Medicine at Mount Sinai, One Gustave L. Levy Place, New York, NY 10029, USA, ⁴Medical Scientist Training Program, Icahn School of Medicine at Mount Sinai, New York, NY 10029, USA, ⁵Department of Pharmacological Sciences, Icahn School of Medicine at Mount Sinai, One Gustave L. Levy Place, New York, NY 10029, USA, ⁶The Mount Sinai Center for RNA Biology and Medicine, Icahn School of Medicine at Mount Sinai, New York, NY 10029, USA and ⁷Department of Pathology, Brigham and Women's Hospital, Harvard Medical School, Boston, MA 02115, USA

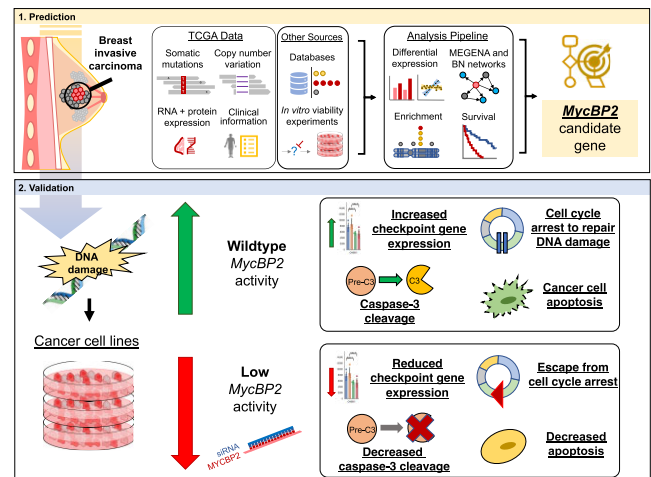
Received April 26, 2023; Editorial Decision June 02, 2023; Accepted June 26, 2023

ABSTRACT

Breast cancer is the most common type of cancer among women worldwide, and it is estimated that 294 000 new diagnoses and 37 000 deaths will occur each year in the United States alone by 2030. Large-scale genomic studies have identified a number of genetic loci with alterations in breast cancer. However, identification of the genes that are critical for tumorigenicity still remains a challenge. Here, we perform a comprehensive functional multi-omics analysis of somatic mutations in breast cancer and identify previously unknown key regulators of breast cancer tumorigenicity. We identify dysregulation of *MYCBP2*, an E3 ubiquitin ligase and an upstream regulator of mTOR signaling, is accompanied with decreased disease-free survival. We validate *MYCBP2* as a key target through depletion siRNA using *in vitro* apoptosis assays in MCF10A, MCF7 and T47D cells. We demonstrate that *MYCBP2* loss is associated with resistance to apoptosis from cisplatin-induced DNA damage and cell cycle changes, and that CHEK1 inhibition can modulate *MYCBP2* activity and caspase cleavage. Furthermore, we show that *MYCBP2* knockdown is associated with transcriptional responses in *TSC2* and in apoptosis genes and interleukins. Therefore, we show that *MYCBP2* is an important genetic target that represents a key node regulating multiple molecular pathways in breast

cancer corresponding with apparent drug resistance in our study.

GRAPHICAL ABSTRACT



INTRODUCTION

Many long-standing pathological studies define breast cancer as a heterogeneous disease through the immunohistochemistry status of various receptors such as estrogen receptor (ER), human epidermal growth factor 2 (HER2/ErbB2) and progesterone receptor (1). Based on this apparent heterogeneity, multiple independent causative genes have been characterized to date that contribute to

*To whom correspondence should be addressed. Tel: +1 212 659 1726; Email: bin.zhang@mssm.edu
Correspondence may also be addressed to Martin J. Walsh. Tel: +1 212 241 9714; Email: martin.walsh@mssm.edu
†The authors wish it to be known that, in their opinion, the first three authors should be regarded as Joint First Authors.

breast cancer prognosis, and they may be attractive options for personalized cancer therapy (2). Recently, the detection of many somatic lesions among breast cancers provides the identification of additional drivers with improved sensitivity and their interconnectivity with specific pathways known to foster human breast tumorigenicity, malignancy, metastasis and their putative relationship to survival (3). Recent multi-omics studies of cancer, such as The Cancer Genome Atlas (TCGA), provide a large body of clinical, genomic, transcriptomic and proteomic data to further determine drug-gable targets for breast cancer through more powerful, integrative approaches (4).

One potential target pathway for breast cancer therapy is the PI3K/AKT/mTOR signaling pathway that is frequently mutated toward gain of function including PIK3CA, AKT, RAS members and other kinases, whereas loss or inactivation of tumor suppressors such as PTEN leads to dysregulated cell growth, tumorigenicity and enhanced survival in multiple breast cancer subtypes (5). Because of their high mutational frequency in breast cancer, multiple inhibitors that target this signaling cascade are currently available or undergoing clinical trials (6). Indeed, the TCGA study showed that PIK3CA, AKT and PTEN dysregulation accounts for 36%, 12% and 22% of breast cancers, respectively (2).

We show a strong correspondence between two genes, *MYCBP2* and *CHEK1*, to the PI3K/AKT/mTOR signaling pathway, with demonstrated capacities to drive breast oncogenesis across multiple breast cancer subtypes, further giving new insights into tumorigenesis and novel targets for cancer therapy. *MYCBP2*, also known as *Myc* binding protein 2 in humans, has a murine orthologue identified as either *Phr1* or *Pam*. Full-length *MYCBP2* encodes a 4640-amino acid protein, previously identified as an E3 ubiquitin ligase, which has been shown to ubiquitinate TSC2, thereby stimulating mTOR activity (6). Interestingly, in other cancer types, including leukemia, melanoma, colon and prostate cancer, *MYCBP2* dysfunction via single-nucleotide polymorphisms has been associated with a poor prognosis (7–9) and corresponds with an earlier presentation of disease (10). *MYCBP2* was identified upstream of pro-apoptotic signaling molecules such as the cellular FLICE-like inhibitory protein (c-FLIP, *CFLAR*) and TNF-related apoptosis-inducing ligand (*TRAIL*) (12). One recent experimental study showed that *MYCBP2* downregulation by miR-17-92 miRNA in multiple uveal melanoma cell lines led to *TRAIL*-mediated resistance to apoptosis, and that *TRAIL* sensitivity and c-FLIP activity are mediated by *MYCBP2*. To date, no experimental studies have been performed on *MYCBP2* in cancer to validate such a function in breast cancer. Beyond the scope of the link of *MYCBP2* to cancer, two studies on *de novo* *MYCBP2* mutations seen in patients with neurodegeneration show that its loss of function may lead to defects in axonal termination resulting in uncontrolled axonal growth and is significantly enriched in autism spectrum disorder (11,12). Additionally, *CHEK1*, also known as checkpoint kinase 1 and a critical Ser/Thr kinase, has been shown to promote cell cycle arrest in response to DNA damage or from *mis*-replicated DNA (13), and has also been shown to phosphorylate *MYCBP2*, based on a large-scale *in vitro* kinase screening assay (14).

Furthermore, *CHEK1* was shown to be upstream of *TP53* and is dysregulated, mutated or phosphorylated among several cancer types, including breast cancer (15,16).

This study investigates the impact of *MYCBP2* mutations on oncogenic processes in breast cancer that include the effects of *MYCBP2* loss in human tumor cell lines. First, by using a novel integrative analysis of the TCGA breast carcinoma data, we identify significant enrichment of *MYCBP2* for somatic single-nucleotide variants (SNVs) among breast cancers. We also discover a significant positive correspondence between *MYCBP2* and mTOR complex gene expression levels. We demonstrate that *CHEK1* is significantly upregulated in breast cancers and also correlates with a poorer prognosis and survival outcomes. Second, through an *in vitro* cell apoptosis assay, we show that human primary cancer cells were more resilient to DNA damage-induced apoptosis when *MYCBP2* is knocked down by siRNA in the presence of the chemotherapeutic agent cisplatin, suggesting that cancers harboring *MYCBP2* loss-of-function mutations correspond with resistance to the drug treatment used. Third, we validate the link between *CHEK1* inhibition and *MYCBP2* knockdown in multiple cancer cell lines and their effects on caspase cleavage, necessary for apoptosis initiation. Lastly, we further characterize the whole transcriptome from *MYCBP2* loss in MCF10A cells before and after siRNA treatment to characterize additional pathways that are modulated by *MYCBP2* in breast cancer tumorigenesis. Collectively, these studies reveal the relationship of the intact *MYCBP2* gene as an important role the E3 ligase, *MYCBP2*, uses to function as an axis for cells to appropriately respond to DNA damage in response to drug therapy, leading to apoptotic cell death. Therefore, by this mechanism, loss of *MYCBP2* in breast cancer can lead to poorer clinical outcomes and response to drug therapy.

MATERIALS AND METHODS

Data sources

Simple somatic mutations for 993 participants with breast invasive carcinoma (BRCA) were collected from an analysis performed by the TCGA Program. Data were generated by whole exome sequencing at the Washington University School of Medicine Genome Sequencing Center using the Illumina Genome Analyzer IIx curated DNA sequencing platform. Somatic mutations were aligned to human reference genome GRCh37 (hg19). Copy number variation (CNV) was collected from 824 samples (722 tumors and 102 adjacent normal samples) from the TCGA-BRCA study with whole exome sequencing performed by the Illumina HiSeq automated sequencing platform. CNVs were generated by the GISTIC algorithm and deposited online in the TCGA data portal. Gene expression data were collected from two sources, including (i) the TCGA-BRCA study with 1087 samples and (ii) the METABRIC study of ER+ breast cancer with 1505 samples (17). The RNA sequencing (RNA-seq) data were normalized by participant age, gender, race and batch number using a mixed effect model. Participant metadata, including disease-free and overall survival, from 1087 participants in the TCGA-BRCA study were collected from the TCGA data portal,

as well as from 1505 participants in the METABRIC study. Short hairpin RNA (shRNA) dropout screens for cancer cell viability from 77 distinct mutational breast cancer cell lines were obtained from the study by Marcotte *et al.* (18) to determine gene oncogenicity.

Gene-level somatic mutational enrichment testing

We tested the enrichment of somatic mutations in each gene using a dN/dS algorithm that compares an estimate of the number of nonsynonymous mutations in a gene with those observed. This method is inspired by a study by Nik-Zainal *et al.* (3) on 560 breast cancers from the TCGA. We first calculate the background rate of synonymous SNV mutations across the entire dataset by counting the number of synonymous mutations against the number of possible synonymous mutations that can be made given the sequence of each gene. We considered different background rates for each 3-mer context of the transition from the reference to alternate allele (e.g. 'ACG' → 'ATG') to estimate 192 different background rates. We then calculate the background synonymous mutation rate of the gene given the number of synonymous sites in the gene by their context. We then adjusted the background mutation rate to a gene-specific mutation rate by the number of synonymous mutations observed in the gene if synonymous mutations were observed in the gene.

$$\begin{aligned} & \text{Exp}(\text{syn mutations}|\text{gene } X) \\ &= \sum_{\substack{i=\text{TTT}, j=\text{TGT} \\ i \rightarrow j|\text{gene } X, i=\text{AAA}, j=\text{ACA}}} \text{observed rate}_{i \rightarrow j|\text{genome synonymous}} \\ & \quad * \text{possible}_{i \rightarrow j|\text{gene } X \text{ synonymous}}, \\ \text{Mutation rate}|\text{gene } X &= \frac{\text{observed mutations}|\text{gene } X}{\text{Exp}(\text{syn mutations}|\text{gene } X)}. \end{aligned}$$

We then estimated the number of nonsynonymous SNV mutations per gene. Using the synonymous mutation rate, we estimate the number of nonsynonymous mutations by mutation type [missense, nonsense, splicing, start codon, 3' untranslated region (UTR), 5' UTR] per gene by multiplying the gene-level synonymous mutation rate by the background nonsynonymous mutation rate of each possible nonsynonymous mutation across the gene given its 3-mer context. This gives us an estimated number of nonsynonymous mutations for the particular gene given its sequence. Since most nonsynonymous mutations are not driver mutations, this expected rate is a good estimate of the model under no selection. Finally, we then use a negative binomial test to generate a probability of the observed number of nonsynonymous mutations in a gene, where p is equal to the estimated nonsynonymous mutation rate of a particular mutation type, n is equal to the number of possible nonsynonymous mutations of that type multiplied by the number of samples and o is equal to the observed number of nonsynonymous mutations.

$$\begin{aligned} & \text{Exp}(\text{nonsyn mutations}|\text{gene } X) \\ &= \sum_{\substack{i=\text{TTT}, j=\text{TGT} \\ i \rightarrow j|\text{gene } X, i=\text{AAA}, j=\text{ACA}}} (\text{Mutation rate}|\text{gene } X) \\ & \quad * \text{observed rate}_{i \rightarrow j|\text{genome nonsyn}} * \text{possible}_{i \rightarrow j|\text{gene } X \text{ nonsyn}}. \end{aligned}$$

$$\begin{aligned} & P(\text{obs}|\text{expexp}|\text{type}) \\ &= \text{NegBinomialTest} \left(\frac{\text{Exp}(\text{nonsyn muts})}{\sum \text{poss. nonsyn}_{\text{gene } X}}, \sum \text{poss. nonsyn}_{\text{gene } X} \right) \\ & \quad * \text{sample size, Obs}(\text{nonsyn muts}), \end{aligned}$$

$$P(\text{obs}|\text{exp}) = \prod_{\text{types}} P(\text{obs}|\text{expexp}|\text{type}).$$

We also used a similar method to calculate enrichment of indels in a particular gene in the BRCA dataset. We used indel data across the entire TCGA dataset of all cancers to estimate a background rate of indels per base without considering context. We calculated separate mutation rates for in-frame, out-of-frame, splice site and UTR indels. We then estimated indel rates per gene given the number of possible coding, splice site and UTR bases, and compared them to the observed number per gene. This generated a separate indel probability per gene, which we combined with the SNV probability.

Construction of gene co-expression and causal networks

The RNASeqV2 data including the RSEM- and MapSplice-derived gene expression levels from the TCGA database (<https://www.cancer.gov/about-nci/organization/ccg/research/structural-genomics/tcga>) were first log-transformed, normalized with quantile normalization and additionally normalized using mixed model correction for batch, tissue source, center, plate, race, gender and age, and then removal of genes with low information was performed by dispersion. A total of 7526 genes were included in the final normalized TCGA-BRCA dataset.

Multiscale embedded gene co-expression network analysis (MEGENA) was used to build gene co-expression networks from the RNA-seq data in the TCGA-BRCA, as described in (19), which constructs a scale-free planar filtered gene co-expression network from Pearson correlation coefficients that has a structure of network hubs and nodes at multiple levels. Bayesian causal gene expression networks (BNs) were built from the normalized RNA-seq and deposited expression quantitative trait locus (eQTL) data across the same 844 tumors in the TCGA-BRCA, as described in (20), where eQTLs provide observed evidence for directed causality for gene co-expression relationships seen in the RNA-seq data.

Identification of key gene network regulators

We applied key driver analysis (KDA) (21) to the MEGENA and BN networks generated from the gene expression data in the TCGA-BRCA, as previously described in this cohort (19), to determine which genes were likely key gene network regulators and critical for the observed transcriptomic changes between breast cancers and adjacent normal samples. In summary, KDA performs enrichment analysis of differentially expressed genes (DEGs) across every gene in a given gene network by examining each gene's N -hop neighbors, where N is the number of hops between a gene and its neighbors.

Cell culture

MCF10A (ATCC CRL-10317™) cells were cultured in Dulbecco's modified Eagle's medium (DMEM)/F-12 (CellGro) with 5% horse serum (Invitrogen), 20 ng/ml epidermal growth factor, 0.5 mg/ml hydrocortisone, 100 ng/ml cholera toxin, 10 µg/ml insulin and 1× penicillin/streptomycin. 293T and MCF7 cells were cultured in DMEM 1× with 10% fetal bovine serum (FBS). T47D cells were maintained in 10% FBS RPMI. Cell culture was performed at 37°C in 5% CO₂ and passaged using 0.25% trypsin/EDTA (Corning).

siRNA transfection and chemical treatment

For the MYCBP2 knockdown with siRNA, MCF10A cells were treated with ON-TARGETplus MYCBP2 and non-target control siRNA (Horizon Dharmacon) using DharmaFECT 1 Transfection Reagent (catalog # T-2001-01). Medium was changed after 5 h. After 48 h of siRNA treatment, cisplatin (Cayman Chemical, catalog # 13119) was added to the cell for 16 h before harvesting the cells for apoptosis and cell cycle analysis assay.

shRNA transfection and chemical treatment

For the MYCBP2 knockdown with shRNA, 293T cells were used to generate lentivirus containing shRNA for scramble or shMycbp2. Briefly, 293T cells were seeded in 10-cm dishes and the following day were co-transfected with the packaging vectors (VSV-G and psPAX2, Addgene #12260) and either shMYCBP2 or shScramble. Medium was changed after 16 h and viruses were collected and filtered through a 0.45-µm filter at 48 and 72 h post-transfection. MCF7 and T47D cells were infected for 24 h and selected with puromycin. After selection was completed and knockdown confirmed by western blotting, cells were treated with rabusertib and dimethyl sulfoxide (DMSO) control for 16 h.

Immunoblotting

Cells were lysed with a common RIPA buffer (25 mM Tris, pH 7.5; 150 mM NaCl; 0.5% sodium deoxycholate; 1% Triton X-100; protease inhibitor) and fractionated by SDS-PAGE gel, and then proteins were transferred to PVDF membranes (Bio-Rad) and blocked at room temperature for an hour with 5% non-fat milk in phosphate-buffered saline (PBS). Primary antibody MYCBP2 (Abcam, catalog # 86078) and CHEK1 (Abcam, catalog # 40866) were added at 1:1000 overnight.

Cell cycle and apoptosis assays

Cell cycle and apoptosis assays were performed on Muse® Cell Analyzer with Annexin V & Dead Cell Assay Kit (catalog # MCH100105) and Cell Cycle Assay Kit (catalog # MCH100106), according to the manufacturer's recommendation. Cells were harvested with trypsin, washed with PBS, fixed with 70% ethanol for 3 h at -20°C (only used for the cell cycle assay), stained with individual dyes from kits and analyzed with Muse® Cell Analyzer.

RNA isolation, cDNA synthesis and RT-qPCR

Total RNA was isolated using the RNeasy Mini Kit (Qiagen, catalog # 74104). One to five micrograms of total RNA was reverse transcribed using iScript™ Reverse Transcription Supermix for reverse transcription quantitative polymerase chain reaction (RT-qPCR; Bio-Rad, catalog # 1708840). qPCR was performed using the GoTaq® qPCR Master Mix (Promega) on the Stratagene Mx3005P Real-Time PCR System (Agilent Technologies, Inc.). Gene expression specific primers used for this study were as follows: GAPDH mRNA was assayed as loading control; MYCBP2 forward primer (5'-3') GGGGACGGATTCTACCCAG; reverse primer (5'-3') ATTGAGCGCAGCGGTATAAAT; CHEK1 forward primer (5'-3') ATATGAAGCGTGC-CGTAGACT; reverse primer (5'-3') TGCCTATGTCTG-GCTCTATTCTG.

Ethics approval and consent to participate

All Institutional Review Board guidelines were followed with human or animal subjects' data when applicable.

RESULTS

Somatic SNVs implicate MYCBP2 as a potential tumor suppressor

To identify novel mutational driver genes in breast cancer, we performed gene-level enrichment analysis of somatic SNVs across all the samples in the TCGA-BRCA. These breast cancers spanned multiple types, as shown in Supplementary Table S1 listing receptor status. Using data from 993 out of 1087 breast cancers with somatic mutation calling data available, we performed gene-level mutational enrichment analysis of all somatic mutations as described in the 'Materials and Methods' section and identified a total of 101 genes significantly enriched for somatic mutations [adjusted *P*-value <0.05 after Benjamini-Hochberg (BH) correction]; a list of all enriched genes identified is provided in Supplementary Table S2. We then performed subsequent downstream filtering to identify novel genes with the strongest evidence, as shown in Figure 1; a list of all enriched genes with filtering annotations is given in Supplementary Table S3. Of these, 45 were in >15 samples (1.5%), a size sufficiently large for further analysis. From these 45 genes, 19 were previously identified as driver genes in public databases (Supplementary Tables S4-S6) and 13 in the literature by PubMed search (Supplementary Table S3), leaving 13 genes for further filtering.

We further filtered these data by differential mRNA expression between breast cancer tumor samples and adjacent normal samples in the TCGA and METABRIC studies (17), leaving 11 genes for further analysis. We then calculated whether mutations in a particular gene were associated with a differential expression signature between mutation carriers and noncarriers, using a false discovery rate (FDR) of 10%, leaving two genes for additional analysis. Finally, we filtered by changes in disease-free survival between carriers of a mutation in a gene and noncarriers using a Kaplan-Meier survival model, using an FDR of 10%, leaving only MYCBP2. We additionally selected MYCBP2 for its

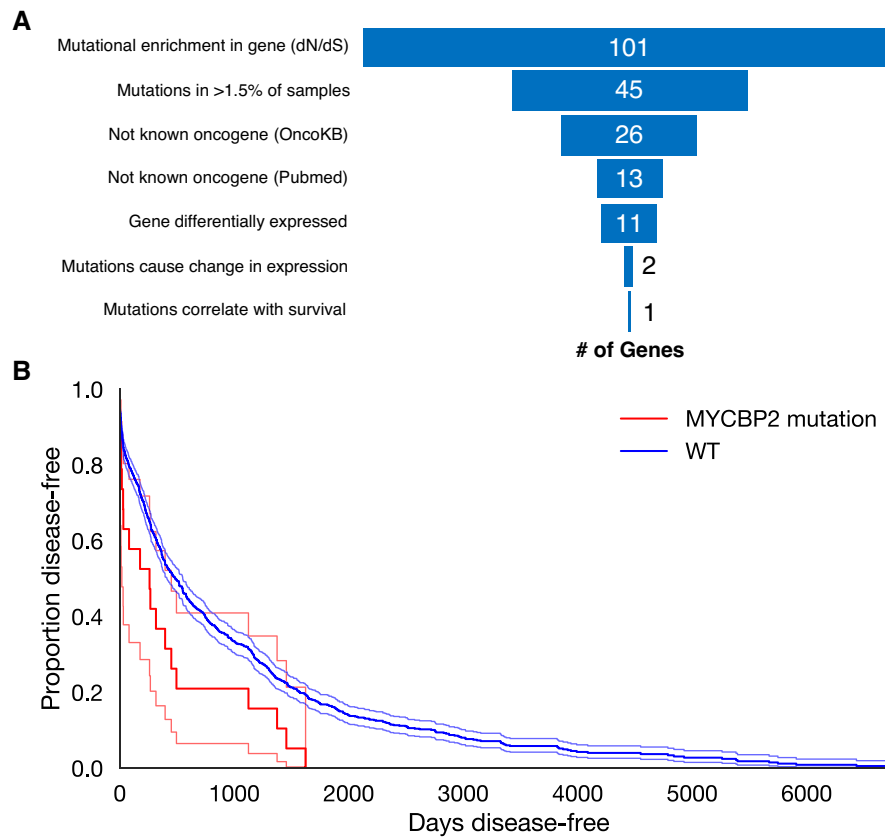


Figure 1. Summary of evidence for *MYCBP2* somatic mutational enrichment. (A) The analytic procedure for identifying *MYCBP2* as a potential mutational driver. (B) Disease-free survival with *MYCBP2* mutations.

potential importance to the mTOR signaling pathway and known link to tumorigenesis.

A list of the significant *P*-values of different filtering analyses for *MYCBP2* is given in Table 1. In the coding region of the dominant transcript expressed of *MYCBP2*, we found significant enrichment of 28 point mutations in 28 samples (2.8%). Of these 28 total mutations, there were 19 missense, 5 stop-gain and 3 silent present on the primary coding transcript for *MYCBP2* (listed in Supplementary Table S7). Three of 28 mutations were present in dbSNP previously (rs745562250, rs150834693, rs770147270), while 25 were not. Functionally among the missense mutations, 11 were predicted deleterious by SIFT (*W4210C*, *M3914T*, *L3910P*, *P3716L*, *C3642W*, *L3477F*, *L3118V*, *D2640H*, *E2013K*, *K1328N*, *V974I*), 6 were predicted functionally significant by MutPred2 (*W4210C*, *M3914T*, *L3910P*, *P3716L*, *C3642W*, *E2013K*) and 2 were predicted likely damaging by PolyPhen (*I3077V*, *E2013K*) (22–24). All of the stop-gain mutations are predicted to be deleterious. We also observed that mutations in *MYCBP2* were significantly associated with poor survival (Cox adjusted *P*-value = 7.4×10^{-3} , Figure 1B). Additionally, we observed a similar nonsignificant correlation between disease-free survival of TCGA participants and *MYCBP2* expression (Cox adjusted *P*-value = 0.126, Supplementary Figure S2B). Finally, we observed that *MYCBP2* had a high burden of shallow deletion CNVs in 416 samples (41.9%) and deep deletions in 9 sam-

Table 1. Summary of changes in *MYCBP2* in the TCGA-BRCA

Test type	<i>MYCBP2</i> <i>P</i> -value
Mutational enrichment	4.22×10^{-8}
SNVs	4.22×10^{-8}
Nonsense	1.4×10^{-3}
Missense	9.9×10^{-3}
Intronic	3.1×10^{-3}
Splice site	1
Start-gain	1
Start-loss	1
Stop-loss	1
UTR	1
Indels	1
DEG (downregulation)	8.3×10^{-24}
Cox survival (w/ expression change)	0.126
Cox survival (w/ mutation status)	7.4×10^{-3}
Cell viability (16)	Nonsignificant

ples (0.9%) from the putative GISTIC data provided by the TCGA Consortium (25); however, there was no difference in survival observed (Cox adjusted *P*-value = 0.943, Supplementary Figure S2C).

To validate somatic mutation enrichment across other cancers, we performed an IntOGen database search for *MYCBP2*, which revealed a variable mutation rate from 0% to 11% across different cancer types (26), as shown in Table 2. Search of COSMIC (27) revealed that

Table 2. Mutation rates of *MYCBP2* across different cancer subtypes from IntOGen database

Cancer type	Mutated samples	% Mutated
Cutaneous melanoma	49	11.11
Lung squamous cell carcinoma	24	10.34
Bladder carcinoma	10	8.16
Stomach adenocarcinoma	14	5.59
Esophageal carcinoma	9	5.48
Head and neck squamous cell carcinoma	17	4.27
Uterine corpus endometrioid carcinoma	14	3.91
Lung adenocarcinoma	17	3.84
Breast carcinoma	24	1.48
Renal clear cell carcinoma	7	1.44

MYCBP2 may be supported as a cancer-causing gene from a large-scale mouse mutagenesis insertional experiment in pancreatic cancer (28); however, none of the mutations observed in the 993 samples were present in the database. A DepMap search for *MYCBP2* shows that the gene may be an essential tumor suppressor in esophageal squamous cell carcinoma by RNAi (P -value: $5.3e-05$, $n = 22$) (29).

To explore the functional pathways in which *MYCBP2* operates, we constructed MEGENA (19) from the TCGA RNA-seq data in the TCGA. A number of gene co-expression modules are significantly enriched for the perturbation signature of *MYCBP2* in the LINCS cohort. As shown in Table 3, the modules enriched for the genes co-downregulated with *MYCBP2* are associated with mitotic cell cycle, while the modules enriched for the genes upregulated by the knockdown of *MYCBP2* are associated with nucleosome and chromatin assembly.

Additionally, we looked at potential pathway genes from a BN, shown in Figure 2A, from the TCGA ER+ breast cancer samples generated in a previous study to evaluate whether or not *MYCBP2* expression is related or causal to genes also in the DNA repair, apoptosis and mitotic cell cycle pathways. As shown in Figure 2B of two-hop network neighbors to *MYCBP2*, many DNA damage repair genes are present, including the *ERCC5* gene (related to UV-mediated DNA damage gene implicated in xeroderma pigmentosum) and the Cdc42 activator *DOCK9*.

As hinted by previous studies investigating *MYCBP2* as a potential DNA damage checkpoint pathway protein, we investigated the association between *MYCBP2* and DNA damage checkpoint proteins *ATM* and *ATR*. As shown in Figure 3A, the mRNA expression profiles of *ATM* and *ATR* are highly correlated with *MYCBP2*, with $r = 0.552$ ($P = 1.3e-68$) and 0.328 ($P = 1.3e-22$), respectively, in the TCGA breast cancer dataset, indicating that *MYCBP2* is co-expressed with *ATM* and *ATR* in breast cancers.

Association of *MYCBP2* with *CHEK1*

CHEK1 is often indicated as a potential driver gene for many cancers (13,15,16,30,31). *CHEK1* has been shown in a large kinase proteomic screen (14) to phosphorylate *MYCBP2* and target it for degradation. As *MYCBP2* and ultimately mTOR are its downstream targets, *CHEK1* may be an important gene for understanding tumorigenesis and for developing novel drugs for breast cancer. In fact, *CHEK1*

inhibitors are already available, with some in clinical trials for cancer (32). *CHEK1*'s role in mTOR pathway dysregulation has yet to be investigated in cancer.

Our analysis shows that *CHEK1* is upregulated in breast cancers compared to adjacent normal tissues, and *CHEK1* expression is important in ER+ cell viability (18) and associated with disease-free survival (Cox P -value = $2.38e-8$) (33). Regarding its potential interaction with *MYCBP2* as a downstream target, we saw a significant negative linear correlation between *CHEK1* and *MYCBP2* gene expression levels (Spearman $r = -0.234$, $P = 6.8 \times 10^{-12}$), as shown in Figure 3A. We also saw a strong negative correlation between *CHEK1* and *TSC2* protein levels (Spearman $r = -0.298$, $P = 2.0e-19$) but also a moderate negative correlation between *CHEK1* and *ATM* protein levels (Spearman $r = -0.200$, $P = 2.5e-9$), given in Figure 3B. Given that the inverse correlation between *TSC2* and mTOR is widely accepted, it is imperative that *CHEK1*'s global effect on the pathway be better elucidated and the role of *MYCBP2* as a mediator of this effect better understood.

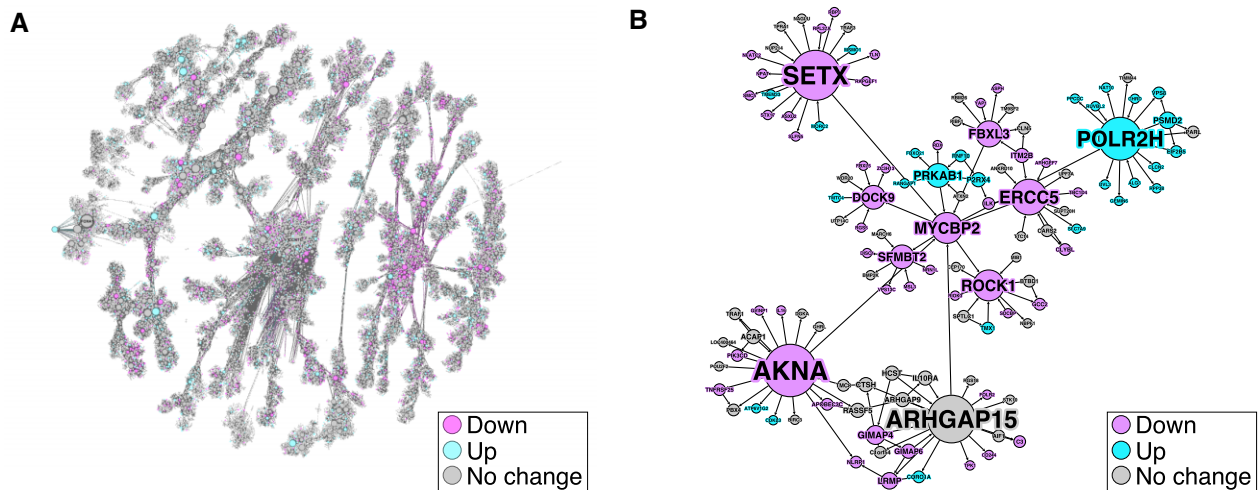
MYCBP2 knockdown makes cells more resistant to apoptosis when exposed to cisplatin

To evaluate the significance of *MYCBP2* loss of function, such as caused by mutations, we performed *in vitro* apoptosis measurements on MCF10A cells before and after *MYCBP2* knockdown with siRNA. Furthermore, since *MYCBP2* is important in the DNA damage response, we also compared the level of apoptosis after cisplatin treatment, which induces DNA damage and cellular stress in a wide variety of cells. Both RT-qPCR and western blot were performed to confirm the *MYCBP2* knockdown efficiency at RNA and protein levels.

As shown in Figure 4A and B, qPCR and western blot of *MYCBP2* after siRNA knockdown show that the expression level is significantly reduced to 33.7% and protein level to 57% of the nontransfected (NT) cells. Follow-up apoptosis assay (Figure 4C and D) by flow cytometry of the knockdown exposed to cisplatin-induced DNA damage compared to transfected controls with mock siRNA showed a large increase in the proportion of live cells and a decrease in apoptotic cells (P -value = 0.0262), which indicates that loss of *MYCBP2* protects the cell from apoptosis upon cisplatin-induced stress. In a separate experiment in both MCF10A and MCF7 cells, we did not observe this protective effect of *MYCBP2* knockdown when exposed to small quantities of DMSO (which does not bind double-stranded DNA) alone (Supplementary Figure S3). Furthermore, we performed a cell cycle assay (Figure 4E) of cells transfected with either siRNA against *MYCBP2* or mock controls in the presence of cisplatin, which showed that cells after knockdown exhibit a faster transition through cell division, with a larger proportion of cells in G0/G1 than S, G2 or M (one-way ANOVA P -value = 1.535×10^{-8}). Furthermore, of cells undergoing replication, knockdown led to larger decreases in the S phase fraction than G2 and M. Therefore, *MYCBP2* loss of function leads to increased tumorigenicity in the presence of induced cell stress by deregulating cell division.

Table 3. Significant MEGENA modules differentially expressed by *MYCBP2* perturbation from the LINCS

Module	Direction	Top GO terms of module	Module size	Overlap	Fold change	FET <i>P</i> -value	FET <i>P</i> -value corr.
M352	Down	Mitotic cell cycle	436	115	-2.06	8.55e-15	4.57e-12
M104	Down	Mitotic cell cycle	1482	285	-1.50	1.48e-13	7.90e-11
M351	Down	Mitotic cell cycle	231	59	-2.00	9.94e-08	5.31e-05
M108	Up	Nucleosome assembly, chromatin assembly	56	24	+3.06	1.31e-07	7.00e-05
M693	Up	Muscle contraction, actin-myosin filament sliding	35	18	+3.68	1.65e-07	8.81e-05
M149	Down	Antigen processing of MHC Class I	62	23	-2.90	1.01e-06	5.39e-04
M12	Down	Immune response, IFN I	283	63	-1.74	6.16e-06	3.29e-03
M705	Down	Mitotic cell cycle	158	40	-1.98	1.35e-05	7.21e-03
M114	Down	Respiratory electron transport chain	243	55	-1.77	1.41e-05	7.53e-03
M259	Down	RNA processing and biosynthesis	76	24	-2.47	1.51e-05	8.06e-03

**Figure 2.** Gene co-expression analysis of *MYCBP2* and related genes in the TCGA breast cancer samples. (A) *MYCBP2* perturbation signature is enriched in the *MYCBP2* centered BN constructed from the TCGA-BRCA samples. (B) BN subnetwork around *MYCBP2*. Pink and blue colors in the figure indicate downregulation and upregulation, respectively, of the gene in perturbed samples compared to baseline.

RNA-seq of MCF10A cells after *MYCBP2* knockdown and cisplatin treatment shows key disease pathway changes

We performed bulk whole transcriptome RNA-seq on MCF10A cells before and after *MYCBP2* siRNA knockdown, both with and without cisplatin exposure. First, as shown in Figure 5A and B, we confirm that *MYCBP2* is downregulated by siRNA inhibition at the transcriptional level [-46.8%, log fold change (FC): -0.912, limma adjusted *P*-value (BH): 2.3×10^{-4}] as well as in response to cisplatin treatment alone (-51.5%, log FC: -1.044, adjusted *P*-value: 6.8×10^{-5}), in line with the results from the qPCR and western blot experiments.

To determine whether cisplatin is acting on *MYCBP2* or on other genes in the pathway, we show that the upstream genes including *ATR* and *CHEK1* are not downregulated in the presence of cisplatin compared to no treatment (*ATR* adjusted *P*-value: 0.15; *CHEK1* adjusted *P*-value: 0.59), even in the presence of si*MYCBP2* (*ATR* adjusted *P*-value: 0.48, *CHEK1* adjusted *P*-value: 0.14), suggesting that the upstream genes from *MYCBP2* are not responsive to cisplatin exposure. Interestingly, two upstream genes *ATR* (adjusted *P*-value: 0.035) and *CHEK1* (adjusted

P-value: 6.0×10^{-4}) are downregulated in the presence of si*MYCBP2* compared to mock, suggesting a potential feedback mechanism with *MYCBP2*.

Nevertheless, we observe downregulation of *MYCBP2* when cells were exposed to cisplatin alone [-27.1%, log FC: -0.456, limma adjusted *P*-value (BH): 0.018], and additional lowering of *MYCBP2* level with cisplatin plus siRNA treatment when compared to siRNA alone (-33.4%, log FC: -0.587, adjusted *P*-value: 5.3×10^{-3}), suggesting that *MYCBP2* is a responsive gene to cisplatin exposure in this pathway. Furthermore, we show that, in line with *MYCBP2*'s predicted E3 ligase inhibitory activity, the downstream apoptosis genes that would usually be downregulated with high *MYCBP2* expression are significantly upregulated in the presence of inhibitory *MYCBP2* siRNA, including pro-survival *CFLAR* (adjusted *P*-value: 0.024) and death receptor TRAIL (*TNFSF10* adjusted *P*-value: 7.75×10^{-4}). Additionally, the downstream genes from *MYCBP2* in the cell growth pathway are also significantly upregulated in the presence of *MYCBP2* siRNA such as *TSC1* (adjusted *P*-value: 1.46×10^{-4}) and *TSC2* (adjusted *P*-value: 7.57×10^{-4}). Critically, the downstream cell cycle genes show

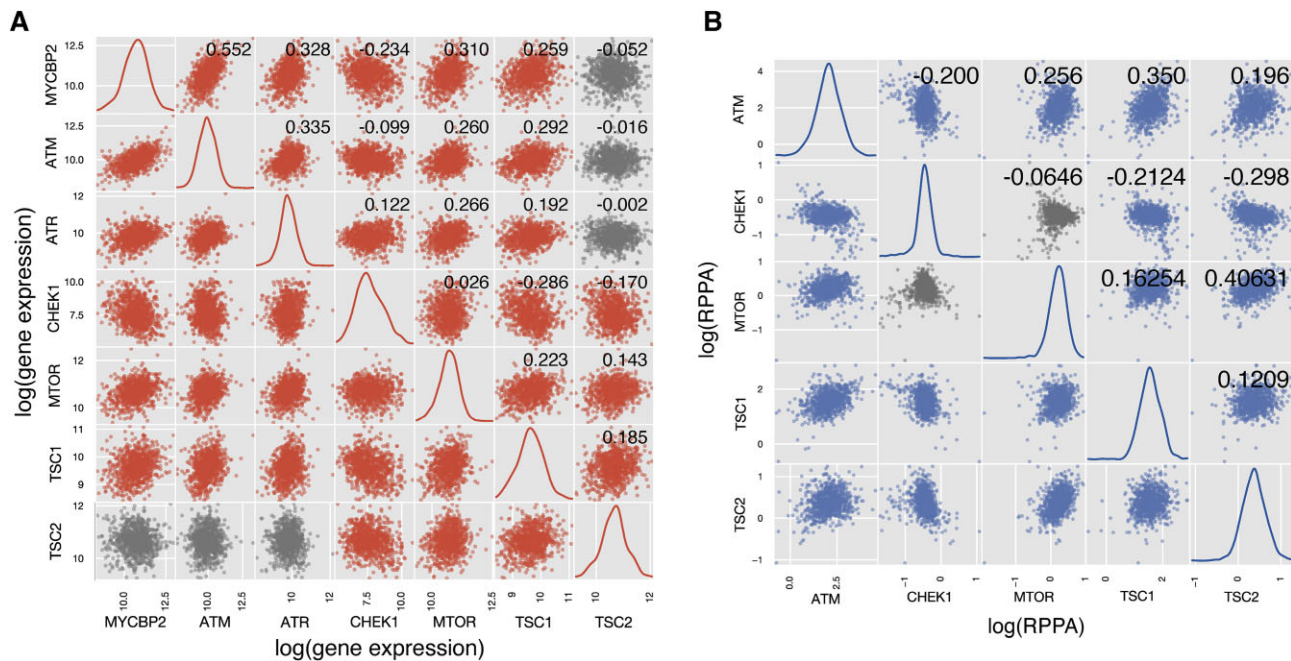


Figure 3. Scatterplot matrix of gene co-expression between MYCBP2, ATM, ATR, CHEK1, MTOR, TSC1 and TSC2 among the TCGA-BRCA samples. Spearman correlation coefficients for gene pairs are given in the upper right corner of the plots as annotated. Colored points indicate that the underlying Spearman correlation is statistically significant (P -value < 0.05), while gray points indicate that there is no correlation (P -value > 0.05). The distribution of gene expression values for each gene is given on the diagonal by their kernel density estimation. (A) Gene co-expression by RNA-seq. (B) Protein co-expression by liquid chromatography–mass spectrometry, where protein expression was averaged across isoforms of each gene.

additional upregulation when exposed to both cisplatin and MYCBP2 siRNA ($TSC1$ adjusted P -value: 0.025, $TSC2$ adjusted P -value: 0.028) but not with cisplatin alone ($TSC1$ adjusted P -value: 0.052, $TSC2$ adjusted P -value: 0.641). Therefore, *MYCBP2* inhibition can dysregulate important genes in the DNA damage, cell cycle and cell growth pathway, while cisplatin's effects on *MYCBP2* activity may also modulate the downstream genes in this pathway.

We also looked at other important apoptosis pathway genes such as direct activators *BAX*, *BAK1*, caspases (*CASP3*, *CASP6*, *CASP7*, *CASP8*, *CASP9*), cytochrome *c* (*CYCS*), *APAF1*, *AIFM1*, *ENDOG*, pro-apoptotic *BMF*, *BAD*, *BIM* (*BCL2L11*), *BID*, *PUMA* (*BBC3*), *HRK*, and apoptosis inhibitors *BCL2A1*, *MCL1* and *BCL-xl* (*BCL2L1*) to measure the degree of *MYCBP2* siRNA knockdown effects on pathway regulation. As shown in Supplementary Figure S1, we saw significant upregulation of pro-apoptotic genes *BMF*, *BIM*, *PUMA* and *HRK*, and significant downregulation of anti-apoptotic genes *BCL2L1* and *MCL1* as well as the pro-apoptotic gene *BID* in the presence of *MYCBP2* siRNA compared to controls (adjusted P -value < 0.05). On the other hand, the direct activators *AIFM1* and *APAF1* are both significantly downregulated in the siRNA plus cisplatin treated group compared to siRNA alone, consistent with the decreased rate of apoptosis we observed, while the expression levels of other direct activators, including the caspases, are not changed. Given that apoptosis decreases in the siRNA knockdown group, it is likely that many apoptosis regulatory genes are upstream of the effects of *MYCBP2*, suggesting that *MYCBP2* is a key intermediate

regulator between regulation and its end effects in DNA damage-mediated apoptosis.

We also looked at important immunomodulatory genes, such as interleukins and important cell surface receptors in cancer, to see whether *MYCBP2* siRNA knockdown may drive changes commonly seen in drug resistance or immune invasion. As expected, knockdown did not lead to a change in expression in estrogen receptor, HER2 receptor or progesterone receptor, suggesting that receptor status also does not change. However, we saw significant downregulation of pro-inflammatory macrophage-related interleukins *IL1A* and *IL1B*, and pro-inflammatory NK-cell activator *IL33*, as well as upregulation of *IL6R*. Taken together, these cytokine changes may facilitate immune evasion by breast cancer and serve as novel biomarkers for cancers transformed by *MYCBP2* deactivation. In addition, other existing biomarkers, such as *CA9*, are nearly absent in *MYCBP2* knockdown cells exposed to cisplatin, while other biomarkers *CXCR4* and *CLU* are significantly upregulated.

Finally, we looked at other E3 ubiquitin ligases that were significantly differentially expressed in *MYCBP2* knockdown cells. Mitogen-activated protein triple kinase 1 (*MAP3K1*) is a Ser/Thr kinase with E3 ligase activity that has been shown to be active in ERK, JNK and NF- κ B pathways. Additionally, loss-of-function mutations in the gene have been previously associated with sensitivity to MEK inhibitors in multiple cancer models (34). We show that *MAP3K1* is significantly upregulated with *MYCBP2* knockdown (adjusted P -value = 1.6×10^{-3}), potentially leading to another resistance mechanism in breast cancers with loss-of-function *MYCBP2* mutations.

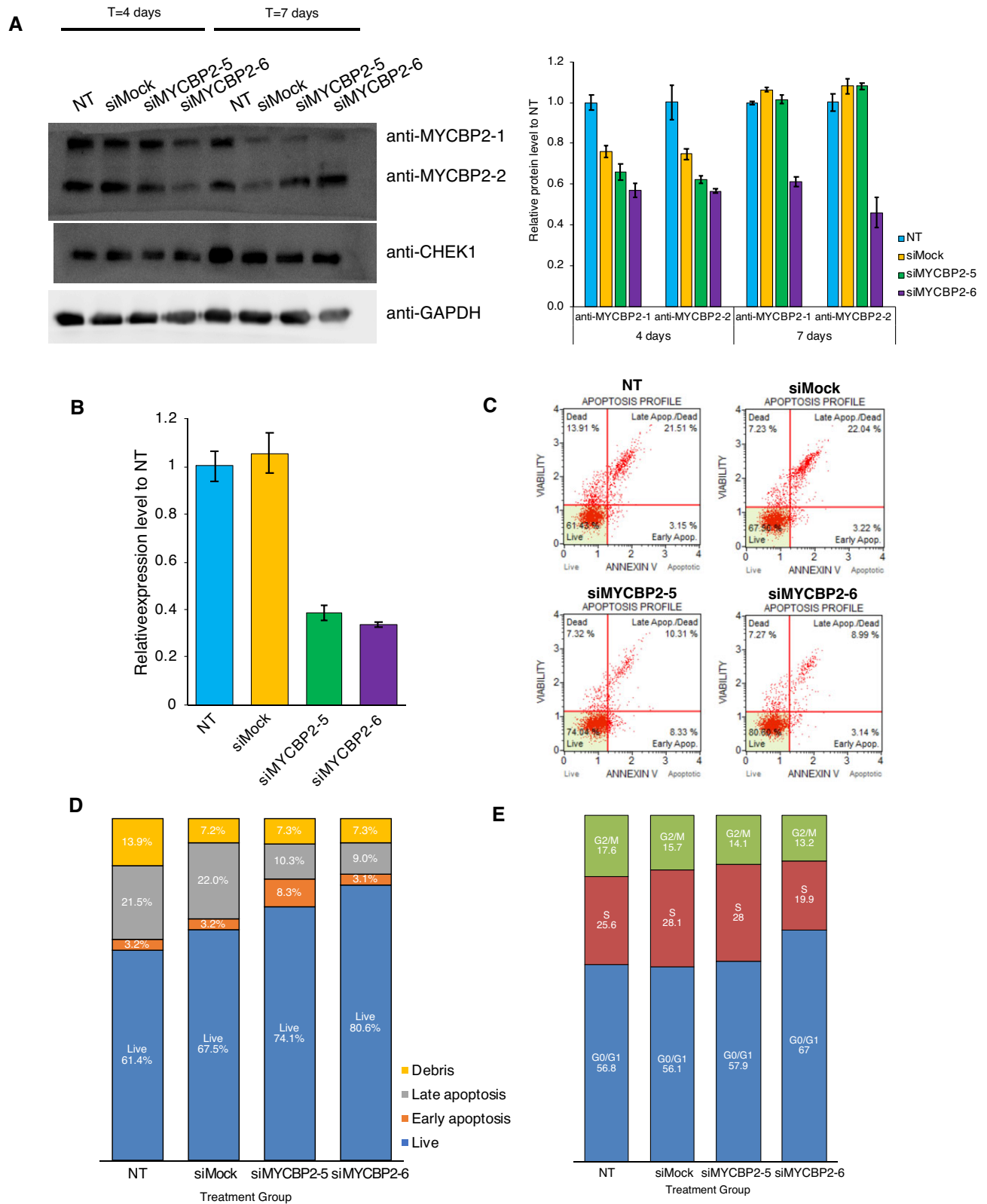


Figure 4. MYCBP2 siRNA inhibition in MCF10A cells exposed to cisplatin. (A) Western blot and protein quantification of MYCBP2 and CHEK1 in NT cells, mock transfected cells and two different siRNAs against MYCBP2 (see the ‘Materials and Methods’ section) after 4 or 7 days of cisplatin exposure. (B) RT-qPCR quantification of MYCBP2 expression level after 4 days of cisplatin exposure. (C, D) Apoptosis assay by flow cytometry of NT, mock transfected and siMYCBP2-(5,6) groups after 4 days of cisplatin exposure. (E) Cell cycle assay by flow cytometry of NT, mock transfected and siMYCBP2-(5,6) groups of MCF10A cells after 4 days of cisplatin exposure.

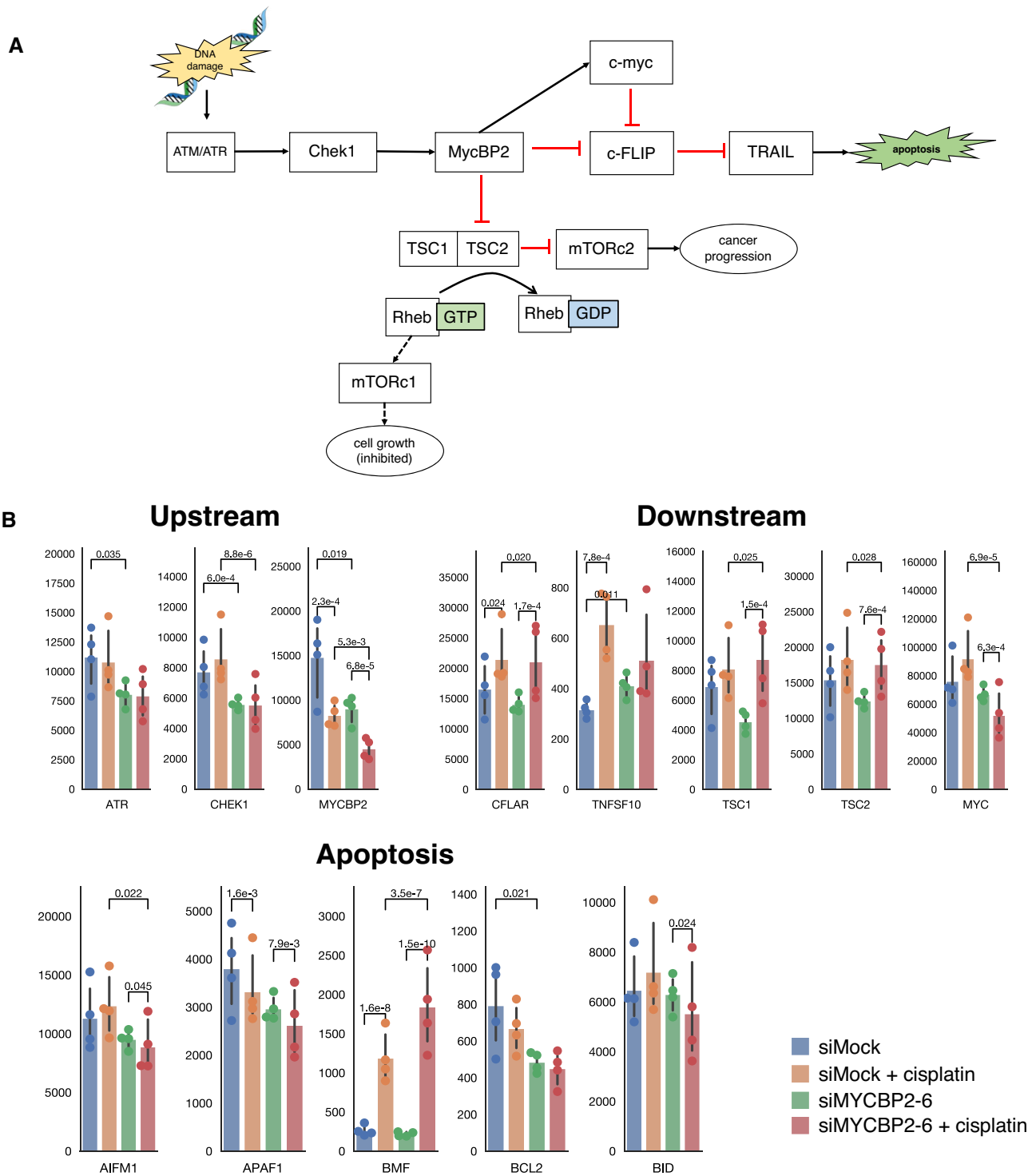


Figure 5. RNA-seq quantification of MYCBP2 knockdown signature on the transcriptome in MCF10A cells. (A) Proposed pathway for MYCBP2 from the previously published literature (6,12,29–31). (B) Gene expression in NT and siMYCBP2-6 exposed cells with and without cisplatin exposure of MYCBP2, proposed upstream genes, downstream genes and apoptosis-related genes.

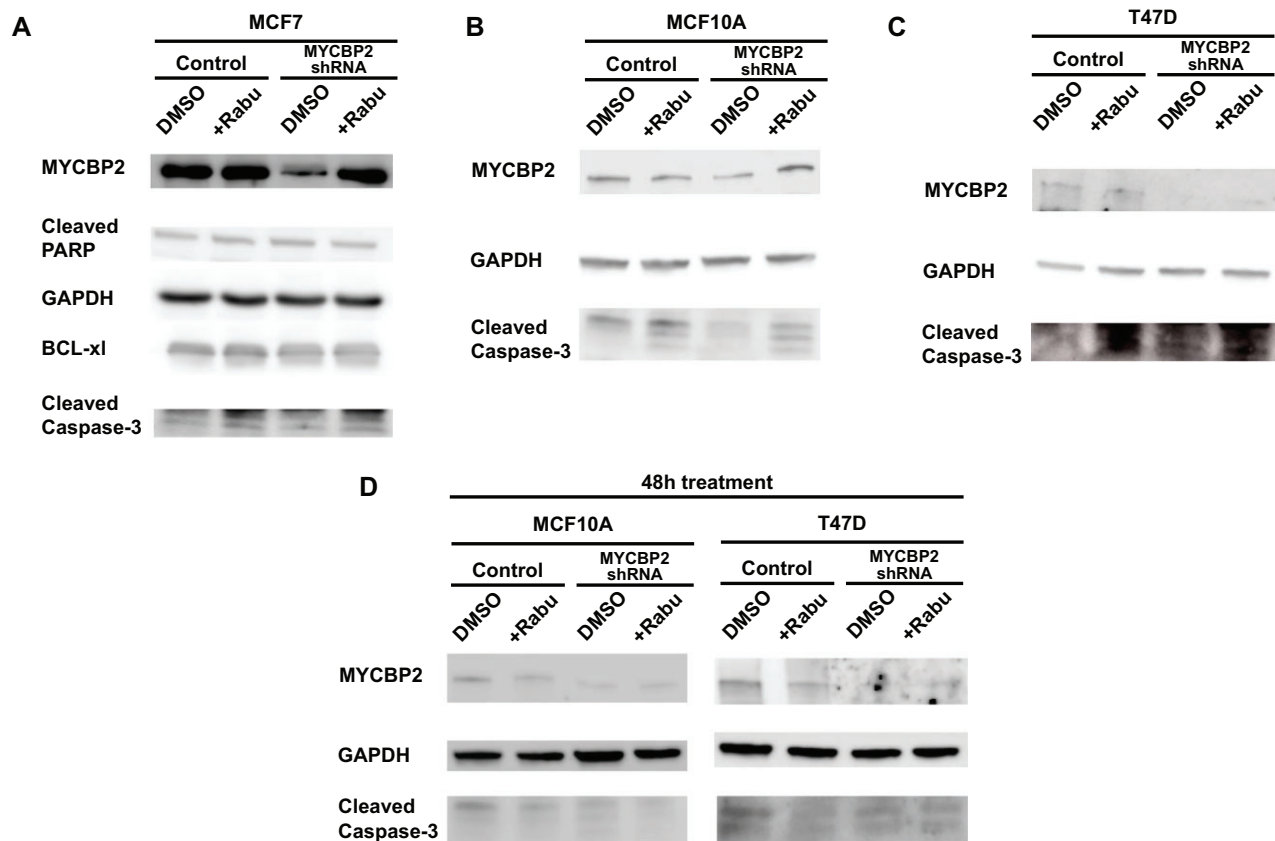


Figure 6. MYCBP2 shRNA knockdown in MCF7, MCF10A and T47D cell lines reduces caspase cleavage and is modulated by CHEK1 inhibition. Cell lines grown in DMSO-containing media, as described in the ‘Materials and Methods’ section, were exposed to no treatment, MYCBP2-targeting shRNA (pLV[shRNA]-EGFP:T2A:Puro-U6>hMYCBP2), rabusterib (4 μ M solution) or a combination of both. Lines in panels (A)–(C) were exposed for 24 h to the mentioned conditions before western blot was performed; lines in panel (D) were exposed for 48 h.

MYCBP2 shRNA knockdown in MCF7, MCF10A and T47D cell lines reduces caspase cleavage and is modulated by CHEK1 inhibition

We performed several western blot experiments, as shown in Figure 6, in cancer cell lines to determine whether MYCBP2 knockdown affects molecular markers of apoptosis in the presence or absence of cell cycle checkpoint modulating agents. We exposed three estrogen receptor-positive breast cancer cell lines (MCF10A, MCF7 and T47D) to MYCBP2 knockdown shRNA both in the presence and in the absence of rabusterib (LY2603618), a known targeted CHEK1 inhibitor drug that has been shown to inactivate the G2/M DNA damage mitotic checkpoint (35,36). The effect of p53 mutations (37) on MYCBP2 activity was also investigated between the choice of T47D (p53 mutant) and MCF7 [p53 wild-type (WT)] cancer cell lines in the experiment.

All three cell lines exposed to MYCBP2 shRNA showed decreased MYCBP2 protein levels on western blot compared to controls, as shown in Figure 6; however, knockdown did not result in complete silencing in MCF10A and MCF7 cell lines. In addition, longer duration exposure to MYCBP2 shRNA results in reduced MYCBP2 levels, as shown in Figure 6D. In general, T47D cells (p53mut) had near-complete silencing of MYCBP2 compared to MCF7

cells (p53 WT), which was further reduced in shRNA knockdown cells, as shown in Figure 6C.

Downstream apoptosis activity was examined by measuring levels of caspase-3 cleavage, a necessary step in the intrinsic mitochondria-driven apoptosis pathway, as well as PARP cleavage and BCL-xl caspase levels. Caspase-3 cleavage was reduced proportionally to MYCBP2 shRNA knockdown in all three cell lines, as shown in Figure 6A–C, suggesting that caspase-3-driven apoptosis is reduced with lower MYCBP2 expression. We did not observe similar reductions in PARP cleavage or BCL-xl in MCF7 cells with MYCBP2 knockdown, as shown in Figure 6A.

In line with previous studies that show CHEK1 is necessary for MYCBP2 phosphorylation and subsequent degradation, exposure of cell lines to rabusterib increases MYCBP2 levels in MCF7, MCF10A and T47D cell lines. Surprisingly, rabusterib increased caspase-3 cleavage in both MYCBP2 knockdown cells and controls at 24 h, as shown in Figure 6A–C, suggesting increasing apoptotic activity with the drug; however, levels of caspase-3 were reduced in cells exposed to shRNA and drug compared to the drug alone. The effects of rabusterib inhibition on caspase-3 cleavage, however, were less significant with longer exposure to the drug, as shown in Figure 6D.

DISCUSSION

Based upon our current findings and from previous studies (5,14,37–39), we devised a comprehensive analysis for how *MYCBP2* (Figure 5A) corresponds with the DNA damage response leading to activation of *ATM/ATR/CHEK1*, to regulate *MYCBP2*, thereby altering cellular growth and proliferation through TSC and mTOR complex genes. Using our analyses to determine the critical nodes within a larger network for human breast cancers, we identify *MYCBP2* to be upstream of pro-apoptotic signaling molecules c-FLIP and TRAIL. Through our detailed transcriptome analysis from RNA-seq, we demonstrated that downstream expression changes in *TSC*, *mTOR*, *c-FLIP* and *TRAIL* correspond with the proposed activity of *MYCBP2* mutations as well as the knockdown signature in the proposed pathway. Therefore, observed changes in cell cycle and apoptotic activity are likely the result of *MYCBP2* knockdown through these effector pathways.

Due to its predicted upstream activity, we hypothesize that gain of *CHEK1* activity can lower *MYCBP2* levels in breast cancer cells. This prospect could be supported, whereby mutations in *MYCBP2* may disrupt *CHEK1* binding or eliminate the *CHEK1* substrate residues, inhibiting its phosphorylation by *CHEK1* and further preventing degradation. Alternatively, new mutations may introduce new *CHEK1* binding sites into *MYCBP2* or stabilize the interaction between *MYCBP2* and *CHEK1* and accelerate its degradation. Further research will elucidate the role of these mutations in binding interactions and activity of these two proteins in the DNA damage response.

CONCLUSION

In this study, we have demonstrated the significant enrichment of somatic mutations within *MYCBP2* across breast and other cancers using the TCGA cohort. We have shown that these mutations correspond with worse clinical outcomes, such as disease-free survival, as well as a distinct gene expression signature in the TCGA. Using *in vitro* experiments in the MCF10A cells, regarded as non-oncogenic human breast epithelial cells, we showed that loss of *MYCBP2* activity increased tumorigenicity by modulating cell cycle arrest leading to reduced apoptosis after DNA damage or cellular stress. After *MYCBP2* knockdown, these cells showed a greater resilience to cisplatin-induced apoptosis, which could explain some of the weaker clinical outcomes observed from our assessment from the TCGA. *MYCBP2* is likely a key regulatory gene modulating cell death in multiple cancer types. After *MYCBP2* transcript knockdown, our transcriptome analysis showed that direct apoptosis activator genes such as *AIFM1* and *APAF1* are down-regulated promoting survival of cancer cells, despite upstream pro-apoptotic signatures in *BAD*, *BIM*, *BCL2* and others. Furthermore, loss of *MYCBP2* activity may modulate cell growth by changing cell cycle activity. Here, we provide strong evidence for the important role of the E3 ligase *MYCBP2* to function in the appropriate response to DNA damage leading to apoptotic cell death, especially along the *CHEK1* pathway. Loss of *MYCBP2* function can therefore lead to drug resistance and further breast tumor growth

and the correspondence to the clinical relationship we revealed.

DATA AVAILABILITY

All raw data, code, analyses and supplementary files for all parts of the manuscript are available at Synapse.org at the following link: <http://dx.doi.org/10.7303/syn25650387>. The raw flow cytometry data can be found at <http://dx.doi.org/10.7303/syn25871487>. The source code is also available at <http://dx.doi.org/10.5281/zenodo.8010736>.

SUPPLEMENTARY DATA

Supplementary Data are available at NAR Cancer Online.

ACKNOWLEDGEMENTS

Authors' contributions: B.Z. perceived the concept and computational study design; R.A.N. carried out the computational study, consulting with and using tools and materials from I.K., W.-M.S. and M.W.; B.Z., M.J.W., A.B.-G., Y.S. and R.N. perceived the *in vitro* experiment design and participated in discussions of the results; A.B.-G. and Y.S. carried out the *in vitro* experiments and subsequent data collection, initial figure generation and initial writeup of *in vitro* results; R.N. wrote the manuscript, including collation and revision of materials from other authors.

FUNDING

National Institutes of Health [R01DK118946, R01GM119189, T32GM007280 and U01AG046170].

Conflict of interest statement. The authors declare no potential conflicts of interest.

REFERENCES

- Wilson,T.R., Yu,J., Lu,X., Spoerke,J.M., Xiao,Y., O'Brien,C., Savage,H.M., Huw,L.-Y., Zou,W., Koeppen,H. *et al.* (2016) The molecular landscape of high-risk early breast cancer: comprehensive biomarker analysis of a phase III adjuvant population. *NPJ Breast Cancer*, **2**, 16022.
- Koboldt,D.C., Fulton,R.S., McLellan,M.D., Schmidt,H., Kalicki-Veizer,J., McMichael,J.F. *et al.* (2012) Comprehensive molecular portraits of human breast tumours. *Nature*, **490**, 61–70.
- Nik-Zainal,S., Davies,H., Staaf,J., Ramakrishna,M., Glodzik,D., Zou,X., Martincorena,I., Alexandrov,L.B., Martin,S., Wedge,D.C. *et al.* (2016) Landscape of somatic mutations in 560 breast cancer whole-genome sequences. *Nature*, **534**, 47–54.
- Zhang,K. and Wang,H. (2015) Cancer Genome Atlas Pan-cancer analysis project. *Chin. J. Lung Cancer*, **18**, 219–223.
- Paplomata,E. and O'Regan,R. (2014) The PI3K/AKT/mTOR pathway in breast cancer: targets, trials and biomarkers. *Ther. Adv. Med. Oncol.*, **6**, 154–166.
- Han,S., Witt,R.M., Santos,T.M., Polizzano,C., Sabatini,B.L. and Ramesh,V. (2008) Pam (protein associated with Myc) functions as an E3 ubiquitin ligase and regulates TSC/mTOR signaling. *Cell. Signal.*, **20**, 1084–1091.
- Ge,Z., Guo,X., Li,J., Hartman,M., Kawasawa,Y.I., Dovat,S. and Song,C. (2015) Clinical significance of high *c-MYC* and low *MYCBP2* expression and their association with *Ikaros* dysfunction in adult acute lymphoblastic leukemia. *Oncotarget*, **6**, 42300–42311.
- Scaravilli,M., Porkka,K.P., Brofeldt,A., Annala,M., Tammela,T.L.J., Jenster,G.W., Nykter,M. and Visakorpi,T. (2015) MiR-1247-5p is overexpressed in castration resistant prostate cancer and targets *MYCBP2*. *Prostate*, **75**, 798–805.

9. Ibáñez, M., Carbonell-Caballero, J., García-Alonso, L., Such, E., Jiménez-Almazán, J., Vidal, E., Barragán, E., López-Pavía, M., Llop, M., Martín, I. *et al.* (2016) The mutational landscape of acute promyelocytic leukemia reveals an interacting network of co-occurrences and recurrent mutations. *PLoS One*, **11**, e0148346.
10. Tricoli, J., Boardman, L.A., Patidar, R., Sindiri, S., Jang, J.S., Walsh, W.D., McGregor, P.M. 3rd, Camalier, C.E., Mehaffey, M.G., Furman, W.L. *et al.* (2018) A mutational comparison of adult and adolescent and young adult (AYA) colon cancer. *Cancer*, **124**, 1070
11. AlAbdi, L., Desbois, M., Rusnac, D.V., Sulaiman, R.A., Rosenfeld, J.A., Lalani, S., Murdock, D.R., Burrage, L.C., Billie Au, P.Y., Towner, S. *et al.* (2023) Loss-of-function variants in MYCBP2 cause neurobehavioural phenotypes and corpus callosum defects. *Brain*, **146**, 1373–1387.
12. Lin, Y., Afshar, S., Rajadhyaksha, A.M., Potash, J.B. and Han, S. (2020) A machine learning approach to predicting autism risk genes: validation of known genes and discovery of new candidates. *Front. Genet.*, **11**, 500064.
13. McNeely, S., Beckmann, R. and Bence Lin, A.K. (2014) CHEK again: revisiting the development of CHK1 inhibitors for cancer therapy. *Pharmacol. Ther.*, **142**, 1–10.
14. Blasius, M., Forment, J.V., Thakkar, N., Wagner, S.A., Choudhary, C. and Jackson, S.P. (2011) A phospho-proteomic screen identifies substrates of the checkpoint kinase Chk1. *Genome Biol.*, **12**, R78.
15. Abdel-Fatah, T.M.A., Middleton, F.K., Arora, A., Agarwal, D., Chen, T., Moseley, P.M. *et al.* (2015) Untangling the ATR–CHEK1 network for prognostication, prediction and therapeutic target validation in breast cancer. *Mol. Oncol.*, **9**, 569–585.
16. Lin, W.Y., Brock, I.W., Connley, D., Cramp, H., Tucker, R., Slate, J. *et al.* (2013) Associations of ATR and CHEK1 single nucleotide polymorphisms with breast cancer. *PLoS One*, **8**, e68578.
17. Curtis, C., Shah, S.P., Chin, S.F., Turashvili, G., Rueda, O.M., Dunning, M.J. *et al.* (2012) The genomic and transcriptomic architecture of 2,000 breast tumours reveals novel subgroups. *Nature*, **486**, 346–352.
18. Marcotte, R., Sayad, A., Brown, K.R., Sanchez-Garcia, F., Reimand, J., Haider, M., Virtanen, C., Bradner, J.E., Bader, G.D., Mills, G.B. *et al.* (2016) Functional genomic landscape of human breast cancer drivers, vulnerabilities, and resistance. *Cell*, **164**, 293–309.
19. Song, W.M. and Zhang, B. (2015) Multiscale embedded gene co-expression network analysis. *PLoS Comput. Biol.*, **11**, e1004574.
20. Katsyv, I., Wang, M., Song, W.M., Zhou, X., Zhao, Y., Park, S., Zhu, J., Zhang, B. and Irie, H.Y. (2016) EPRS is a critical regulator of cell proliferation and estrogen signaling in ER+ breast cancer. *Oncotarget*, **7**, 69592–69605.
21. Zhang, B. and Zhu, J. (2013) Identification of key causal regulators in gene networks. In: *Proceedings of the World Congress on Engineering 2013*. International Association of Engineers, pp. 1309–1312.
22. Vaser, R., Adusumalli, S., Leng, S.N., Sikic, M. and Ng, P.C. (2016) SIFT missense predictions for genomes. *Nat. Protoc.*, **11**, 1–9.
23. Pejaver, V., Urresti, J., Lugo-Martinez, J., Pagel, K.A., Lin, G.N., Nam, H.J., Mort, M., Cooper, D.N., Sebat, J., Iakoucheva, L.M. *et al.* (2020) Inferring the molecular and phenotypic impact of amino acid variants with MutPred2. *Nat. Commun.*, **11**, 5918.
24. Adzhubei, I., Jordan, D.M. and Sunyaev, S.R. (2013) Predicting functional effect of human missense mutations using PolyPhen-2. *Curr. Protoc. Hum. Genet.*, **76**, 7.20.1–7.20.41.
25. Grossman, R.L., Heath, A.P., Ferretti, V., Varmus, H.E., Lowy, D.R., Kibbe, W.A. and Staudt, L.M. (2016) Toward a shared vision for cancer genomic data. *New Engl. J. Med.*, **375**, 1109–1112.
26. Gonzalez-Perez, A., Perez-Llamas, C., Deu-Pons, J., Tamborero, D., Schroeder, M.P., Jene-Sanz, A. *et al.* (2013) IntOGen-mutations identifies cancer drivers across tumor types. *Nat. Methods*, **10**, 1081–1084.
27. Forbes, S.A., Beare, D., Gunasekaran, P., Leung, K., Bindal, N., Boutselakis, H., Ding, M., Bamford, S., Cole, C., Ward, S. *et al.* (2015) COSMIC: exploring the world's knowledge of somatic mutations in human cancer. *Nucleic Acids Res.*, **43**, D805–D811.
28. Pérez-Mancera, P.A., Rust, A.G., Van Der Weyden, L., Kristiansen, G., Li, A., Sarver, A.L., Silverstein, K.A.T., Grützmann, R., Aust, D., Rümmele, P. *et al.* (2012) The deubiquitinase USP9X suppresses pancreatic ductal adenocarcinoma. *Nature*, **486**, 266–270.
29. Corsello, S.M., Nagari, R.T., Spangler, R.D., Rossen, J., Kocak, M., Bryan, J.G., Humeidi, R., Peck, D., Wu, X., Tang, A.A. *et al.* (2020) Discovering the anticancer potential of non-oncology drugs by systematic viability profiling. *Nat. Cancer*, **1**, 235–248.
30. Liu, B., Qu, J., Xu, F., Guo, Y., Wang, Y., Yu, H. and Qian, B. (2015) MiR-195 suppresses non-small cell lung cancer by targeting CHEK1. *Oncotarget*, **6**, 9445–9456.
31. Sinha, S., Singh, R.K., Bhattacharya, N., Mukherjee, N., Ghosh, S., Alam, N., Roy, A., Roychoudhury, S., Panda, C.K. *et al.* (2011) Frequent alterations of LOH11CR2A, PIG8 and CHEK1 genes at chromosomal 11q24.1–24.2 region in breast carcinoma: clinical and prognostic implications. *Mol. Oncol.*, **5**, 454–464.
32. Mohni, K.N., Kavanaugh, G.M. and Cortez, D. (2014) ATR pathway inhibition is synthetically lethal in cancer cells with ERCC1 deficiency. *Cancer Res.*, **74**, 2835–2845.
33. Gao, J., Aksoy, B.A., Dogrusoz, U., Dresdner, G., Gross, B., Sumer, S.O., Sun, Y., Jacobsen, A., Sinha, R., Larsson, E., Cerami, E. *et al.* (2013) Integrative analysis of complex cancer genomics and clinical profiles using the cBioPortal. *Sci. Signal.*, **6**, pii.
34. Xue, Z., Vis, D.J., Bruna, A., Sustic, T., van Wageningen, S., Batra, A.S. *et al.* (2018) MAP3K1 and MAP2K4 mutations are associated with sensitivity to MEK inhibitors in multiple cancer models. *Cell Res.*, **28**, 719–729.
35. Witkiewicz, A.K., Chung, S., Brough, R., Vail, P., Franco, J., Lord, C.J. *et al.* (2018) Targeting the vulnerability of RB tumor suppressor loss in triple-negative breast cancer. *Cell Rep.*, **22**, 1185–1199.
36. Wang, F.Z., Fei, H.R., Cui, Y.J., Sun, Y.K., Li, Z.M., Wang, X.Y. *et al.* (2014) The checkpoint 1 kinase inhibitor LY2603618 induces cell cycle arrest, DNA damage response and autophagy in cancer cells. *Apoptosis*, **19**, 1389–1398.
37. Pabla, N., Huang, S., Mi, Q.S., Daniel, R. and Dong, Z. (2008) ATR–Chk2 signaling in p53 activation and DNA damage response during cisplatin-induced apoptosis. *J. Biol. Chem.*, **283**, 6572–6583.
38. Grill, B., Murphey, R.K. and Borgen, M.A. (2016) The PHR proteins: intracellular signaling hubs in neuronal development and axon degeneration. *Neural Dev.*, **11**, 8.
39. Yu, J.W. and Shi, Y. (2008) FLIP and the death effector domain family. *Oncogene*, **27**, 6216–6227.